Physics in Medicine & Biology

IPEM Institute of Physics and Engineering in Medicine

PAPER • OPEN ACCESS

Optimized *I*-values for use with the Bragg additivity rule and their impact on proton stopping power and range uncertainty

To cite this article: Esther Bär *et al* 2018 *Phys. Med. Biol.* **63** 165007

IOP Publishing Phys. Med. Biol. 63 (2018) 165007 (17pp) https://doi.org/10.1088/1361-6560/aad312

Physics in Medicine & Biology

IPEM Institute of Physics and Engineering in Medicine

OPEN ACCESS

PAPER

Optimized *I*-values for use with the Bragg additivity rule and their impact on proton stopping power and range uncertainty

Esther Bär[1,2], **Pedro Andreo**[3], **Arthur Lalonde**[4], **Gary Royle**[2] **and Hugo Bouchard**[4]

[1] Chemical, Medical and Environmental Science Department, National Physical Laboratory, Hampton Road, Teddington TW11 0LW, United Kingdom
[2] Department of Medical Physics and Biomedical Engineering, University College London, Gower Street, London WC1E 6BT, United Kingdom
[3] Dept of Medical Radiation Physics and Nuclear Medicine, Karolinska University Hospital, SE-171 76 Stockholm, Sweden
[4] Department of Physics, Université de Montréal, 2900 boul. Édouard-Montpetit, Montréal QC H3T 1J4, Canada

E-mail: esther.baer.11@ucl.ac.uk **and** h.bouchard@umontreal.ca

Keywords: particle therapy, mean excitation energy, range uncertainty

RECEIVED
27 March 2018

REVISED
4 July 2018

ACCEPTED FOR PUBLICATION
12 July 2018

PUBLISHED
10 August 2018

Abstract

Novel imaging modalities can improve the estimation of patient elemental compositions for particle treatment planning. The mean excitation energy (*I*-value) is a main contributor to the proton range uncertainty. To minimize their impact on beam range errors and quantify their uncertainties, the currently used *I*-values proposed in 1982 are revisited. The study aims at proposing a new set of optimized elemental *I*-values for use with the Bragg additivity rule (BAR) and establishing uncertainties on the optimized *I*-values and the BAR.

We optimize elemental *I*-values for the use in compounds based on measured material I-values. We gain a new set of elemental *I*-values and corresponding uncertainties, based on the experimental uncertainties and our uncertainty model. We evaluate uncertainties on *I*-values and relative stopping powers (RSP) of 70 human tissues, taking into account statistical correlations between tissues and water. The effect of new *I*-values on proton beam ranges is quantified using Monte Carlo simulations.

Our elemental *I*-values describe measured material *I*-values with higher accuracy than ICRU-recommended *I*-values (RMSE: 6.17% (ICRU), 5.19% (this work)). Our uncertainty model estimates an uncertainty component from the BAR to 4.42%. Using our elemental *I*-values, we calculate the *I*-value of water as 78.73 $\pm$ 2.89 eV, being consistent with ICRU 90 (78 $\pm$ 2 eV). We observe uncertainties on tissue *I*-values between 1.82-3.38 eV, and RSP uncertainties between 0.002%–0.44%. With transport simulations of a proton beam in human tissues, we observe range uncertainties between 0.31% and 0.47%, as compared to current estimates of 1.5%.

We propose a set of elemental *I*-values well suited for human tissues in combination with the BAR. Our model establishes uncertainties on elemental *I*-values and the BAR, enabling to quantify uncertainties on tissue *I*-values, RSP as well as particle range. This work is particularly relevant for Monte Carlo simulations where the interaction probabilities are reconstructed from elemental compositions.

1. Introduction

Radiotherapy with protons has become the preferred treatment technique for various indications. The main advantage of radiotherapy with protons lies in their favorable dose deposition pattern as compared to photons. Protons deposit most of their energy at the end of their track, forming a well defined dose peak, the so called Bragg peak. The Bragg peak is followed by a steep dose fall off, with practically zero dose beyond its location. An important part of treatment planning with protons or heavier ions is the prediction of the position of this Bragg peak within the patient. In clinical practice, this position is predicted based on a single-energy CT (SECT) scan of the patient. The acquired CT numbers are converted into the needed quantities. These quantities can be relative stopping powers (RSPs) or elemental compositions for analytical (Schneider *et al* 1996) or Monte Carlo (MC)

dose calculation techniques (Schneider *et al* 2000). Since SECT does not provide enough information to predict these parameters accurately, uncertainties are introduced (Schaffner and Pedroni 1998). These uncertainties are taken into account during treatment planning by adding uncertainty margins to the treatment volume.

In recent years, dual-energy CT (DECT) was explored by several groups. DECT provides additional information and therefore has the potential to increase accuracy in the prediction of tissue parameters (Alvarez and Macovski 1976, Torikoshi *et al* 2003, Williamson *et al* 2006, Bazalova *et al* 2008). Different formalisms exist to either predict RSP values (Yang *et al* 2010, Hünemohr *et al* 2014a, Bourque *et al* 2014, Möhler *et al* 2016, Taasti *et al* 2016) or elemental compositions (Landry *et al* 2013, Hünemohr *et al* 2014b, Lalonde and Bouchard 2016, Lalonde *et al* 2017) from a DECT scan. Some of these formalisms have been successfully validated in animal tissue studies (Taasti *et al* 2017, Bär *et al* 2018, Möhler *et al* 2018, Xie *et al* 2018), and it was shown that uncertainties on the beam range prediction can be reduced by 0.34% using DECT (Bär *et al* 2017, Bär *et al* 2018).

With DECT being on the edge of clinical implementation for radiotherapy, one major remaining source of uncertainty lies in the determination of the mean excitation energy, or *I*-value, of patient tissues. The portion of range uncertainties arising from *I*-values was previously estimated to 1.5% (Paganetti 2012). A recent survey (Taasti *et al* 2018) shows that particle therapy facilities apply a relative range margin or 3.5%, which was recommended by Paganetti and includes the before mentioned 1.5% portion coming from the *I*-values.

In practice, the *I*-values for compounds are calculated from elemental *I*-values using the Bragg additivity rule (BAR). Current clinically used elemental *I*-values were estimated by Berger and Seltzer in 1982 (Berger and Seltzer 1982), and in 1984 those values were adapted as recommendation in the ICRU report 37 (ICRU 1984), and later taken over for the use in proton and ion radiotherapy in ICRU report 49 (ICRU 1993). Berger and Seltzer (1982) used a large set of different compound *I*-values to estimate the elemental *I*-values for elements in compounds. The compound *I*-values they used were taken from previous publications using two different methods. Firstly, they took measured stopping power data (Thompson 1952, Tschalär and Bichsel 1968, Nordin and Henkelman 1979, Bichsel and Hilko 1981) from which they derived the compound *I*-values and their uncertainties according to equations 3.9 and 3.11 in ICRU 37 (ICRU 1984). Secondly, they took calculated compound *I*-values from dipole oscillator-strength distributions or dielectric-response functions (Bader *et al* 1956, Zeiss *et al* 1977, Thomas and Meath 1977, Ashley *et al* 1978, Painter *et al* 1980, Jhanwar *et al* 1981). Details of how those *I*-values were derived from the oscillator-strength and dielectric data can be found in ICRU 37. Based on those compound data, they estimated two sets of elemental *I*-values to use in compounds in combination with the BAR, one set for gases and one set for liquids and solids. It is important to note that the *I*-value of an element or a molecule depends on whether it is unbound or bound, and the type of chemical bond. Hence, elemental *I*-values for the use in compounds are different from *I*-values of unbound elements. Since the elemental *I*-values of Berger and Seltzer were recommended by the ICRU, they are in clinical use to calculate the *I*-values of compound materials such as human body tissues.

The estimation of range uncertainties arising from *I*-values has always been challenging. Andreo (2009) showed differences in beam ranges of 0.3 g cm^{-2} for a 122 MeV proton beam when the water *I*-value varies from 67 eV to 80 eV, covering the variety of values proposed in literature. Differences get larger when considering different tissue types or different particle species. Besemer *et al* (2013) performed a variation study that uniformly varies the tissue *I*-values, and evaluated the influence on patient dose distributions. They showed that a 10% variation of *I*-values influences the R_{80} beam range by up to 4.8 mm, and resulting dose distributions by up to 3.5%. Although the uncertainties on *I*-values can be relatively high, two studies by Yang *et al* (2012) and De Smet *et al* (2018) suggest that the resulting RSP values are much lower since correlations between water and medium need to be taken into account. Another study by Doolan *et al* (2016) investigated the influence of different correction terms to the Bethe formula on the calculated stopping power. They suggest to use the *I*-value as a free parameter to optimize according to which corrections to the Bethe formula are used, in order to avoid systematic errors on RSP values. Recent work suggests the estimation of a patient specific tissue *I*-value from MRI imaging (Sudhyadhom 2017).

It was shown in recent studies that accurate knowledge of the *I*-values allows for reduced uncertainties of the water-to-air stopping power ratio of carbon ion beams, an important quantity in reference dosimetry (Sánchez-Parcerisa *et al* 2012). Furthermore, *I*-values are one of the main sources of uncertainties in water equivalent range calculations and beam transport models for protons and heavier ions (Zhang *et al* 2010, Paul and Sánchez-Parcerisa 2013).

The aim of this work is to revise the currently used elemental *I*-values. We believe that a revision of *I*-values and an addition to the pioneer work by Berger and Seltzer is necessary for the following reasons:

1. The original publication by Berger and Seltzer does not give details on how exactly the elemental *I*-values are derived from the given compound measurements, making it difficult to reproduce their values.
2. Since the work of Berger and Seltzer, several new stopping power measurements were performed (Bichsel and Hiraoka 1992, Hiraoka *et al* 1993, 1994, Bichsel *et al* 2000, Kumazaki *et al* 2007) which can be included into the estimation of elemental *I*-values for the use in compounds.

3. The values by Berger and Seltzer are quoted without uncertainty budget, which makes it difficult to estimate resulting uncertainties on RSPs and ranges.

In order to revise the currently applied I-values, we develop a mathematical model to find, based on old and new measurement data, an optimal set of elemental I-values for the use in compounds. Furthermore, our model establishes an uncertainty budget on our newly found set of elemental I-values as well as on the BAR. Our uncertainty budget allows the propagation of uncertainties from elemental I-values to relative stopping powers of tissues and ultimately to beam ranges, to give a rigorous estimate of range uncertainties arising from I-values.

2. Materials and methods

2.1. Optimal elemental I-values to estimate compound I-values

The stopping power of charged particles in a medium m is described by the Bethe formula (Bethe 1930). We can formulate the RSP in terms of relative electron density ρ_e and stopping number L as

$$S_{\text{med}} = \rho_e \frac{L_{\text{med}}}{L_w} \tag{1}$$

where L_{med} and L_w are the stopping numbers of the medium and water, respectively. The stopping number of an arbitrary medium is expressed as

$$L = \ln\left(\frac{2m_e c^2 \beta^2}{1-\beta^2}\right) - \beta^2 - \ln(I), \tag{2}$$

with m_e the electron mass, c the speed of light, β is the velocity in units of c, and I is the mean excitation energy of the medium. Please note that the Bethe formula is valid for protons and heavier ions, and that the I-value is a tissue-specific parameter and does not depend on the particle type. The herein presented values are hence valid for electrons, protons and heavier ions.

Let us define a series of M media indexed by $i = 1, \ldots, M$ consisting of N elements and with given elemental weights $w_{\text{med},ij}$, with $j = 1, \ldots, N$. The Bragg additivity rule (BAR) allows an estimation of the mean excitation energy $I_{\text{med},i}$ of the ith medium using the weighted sum of the logarithmic elemental mean excitation energies:

$$\ln I_{\text{med},i} \approx \sum_{j=1}^{N} \lambda_{\text{med},ij} \ln I_{\text{med},j} \tag{3}$$

where $\lambda_{\text{med},ij}$ is the fraction of electrons from the jth element in the ith medium and given by

$$\lambda_{\text{med},ij} = \frac{w_{\text{med},ij}\frac{Z_j}{A_j}}{\left(\frac{Z}{A}\right)_{\text{med},i}} \tag{4}$$

with Z_j and A_j the atomic number and molar mass of the jth element, and $\left(\frac{Z}{A}\right)_{\text{med},i}$ is the number of electrons per unit mass in the medium (in mol/g). Using matrix notation, the BAR can be written as the following estimator

$$\mathbf{y}_{\text{med}} \approx \hat{\mathbf{y}}_{\text{med}} \equiv \mathbf{\Lambda}_{\text{med}} \hat{\mathbf{y}}_{\text{elem}} \tag{5}$$

where $\mathbf{y}_{\text{med}}$ is a $M \times 1$-dimensional array containing the logarithm of experimental I-values and $\hat{\mathbf{y}}_{\text{elem}}$ is an array of dimension $N \times 1$ containing the optimized logarithm of elemental I-values for use with the BAR defined as

$$\hat{y}_{\text{elem},j} \equiv \ln \hat{I}_j. \tag{6}$$

The matrix $\mathbf{\Lambda}_{\text{med}}$ of dimension $M \times N$ contains the fractions of electrons for the respective materials and its elements are written as $\lambda_{\text{med},ij}$, corresponding tor the ith medium and jth element.

We propose to determine a new set of optimized elemental I-values, i.e. $\hat{I}_j$, by finding the weighted least square solution of equation (5). To take measurement and model uncertainties into account, we introduce weighting factors accounting for uncertainties:

$$\omega_i = \frac{1}{\sqrt{u_{\text{med},i}^2}} \tag{7}$$

with $u_{\text{med},i}$ being the relative uncertainty of the I-value experimental measurement of the ith medium. Note that because these uncertainties represent the absolute uncertainty of the natural logarithm of the I-value, they are reported in relative uncertainty on the I-value (i.e. in %). These weighting factors multiply individually both sides of the equation system (5) to account for uncertainties, leading to a new equation system

$$\tilde{\mathbf{y}}_{\text{med}} \approx \tilde{\mathbf{\Lambda}}_{\text{med}} \hat{\mathbf{y}}_{\text{elem}} \tag{8}$$

where the elements of $\tilde{\mathbf{y}}_{\text{med}}$ are $\omega_i y_{\text{med},i}$ and the elements of $\tilde{\mathbf{\Lambda}}_{\text{med}}$ are $\omega_i \lambda_{\text{med},ij}$. We can now find the least square solution to equation (8):

$$\begin{aligned}\hat{\mathbf{y}}_{\text{elem}} &= \left(\tilde{\mathbf{\Lambda}}_{\text{med}}^{\text{T}}\tilde{\mathbf{\Lambda}}_{\text{med}}\right)^{-1}\tilde{\mathbf{\Lambda}}_{\text{med}}^{\text{T}}\tilde{\mathbf{y}}_{\text{med}} \\ &= \tilde{\mathbf{M}}\tilde{\mathbf{y}}_{\text{med}},\end{aligned} \tag{9}$$

with $\hat{\mathbf{y}}_{\text{elem}}$ being the estimation of the optimized logarithmic elemental I-values and $\tilde{\mathbf{M}}$ a projection matrix (from the measurement to the solution) defined to ease the notation. To find the uncertainties on elemental I-values, we construct the covariance matrix of $\hat{\mathbf{y}}_{\text{elem}}$ as follows:

$$\mathbf{V}\left(\hat{\mathbf{y}}_{\text{elem}}\right) = \tilde{\mathbf{M}}V\left(\tilde{\mathbf{y}}_{\text{med}}\right)\tilde{\mathbf{M}}^{\text{T}} + u_{\text{BAR}}^2\mathbb{1}_{N\times N}, \tag{10}$$

with $\mathbf{V}\left(\tilde{\mathbf{y}}_{\text{med}}\right)$ being the covariance matrix on measured material I-values with each line weighted by its corresponding ω_i. Note that because the measurements are assumed independent, $\mathbf{V}\left(\tilde{\mathbf{y}}_{\text{med}}\right)$ is diagonal.

Equation (10) is defined by combining two terms. The first one is obtained by applying the rule of uncertainty propagation on equation (9), since the Jacobian $\left(\partial\hat{\mathbf{y}}_{\text{elem}}/\partial\tilde{\mathbf{y}}_{\text{med}}\right)$ is the projection matrix $\tilde{\mathbf{M}}$. The second term is added to account for the model uncertainty. Indeed, the rule of uncertainty propagation can only yield accurate uncertainty estimations if the model is exact. Because the BAR is not completely accurate, it is judicious to add a model uncertainty component u_{BAR}^2 affecting each optimized values individually and in an independent manner. This way, we divide the uncertainties involved in the estimation of elemental I-values into experimental type A uncertainties and model-related type B uncertainties. The resulting $\mathbf{V}\left(\hat{\mathbf{y}}_{\text{elem}}\right)$ is a non-diagonal square matrix of dimensions $N \times N$ accounting for statistical correlations in the solution.

The solution expressed in equation (9) using indirectly measured (from stopping power measurements) and calculated (from dipole-oscillator and dielectric data) compound I-value data yields a new set of elemental I-values $\hat{I}_j$ for use with the BAR. The required I-values were taken from different sources as listed in table 1. They include the data provided in ICRU report 37, table 5.3 of ICRU (1984) and more recent publications. The materials, elemental compositions and corresponding I-values can be found in tables A1 and A2. This formalism starts with compound I-values, as extracted from stopping power measurements, dipole-oscillator and dielectric data. Like Berger and Seltzer, we divide the data into two groups: (1) gases; (2) liquids and solids. For gases, the data used in this work are the same than the ones used by Berger and Seltzer (1982) to determine the recommended elemental I-values in ICRU report 37. For liquids and solids, we added data published in recent literature (see table 1, numbers 11–15). In total, we use 74 liquids and solids for calibration, including six different I-values for water (Thompson 1952, Nordin and Henkelman 1979, Bichsel and Hiraoka 1992, Bichsel *et al* 2000, Kumazaki *et al* 2007, Emfietzoglou *et al* 2009). We refer to this method as a calibration because calculated or measured compound I-values are used to derive model parameters (elemental I-values) that will be used for the prediction of unknown values, such as I-values in patient tissues. The elemental I-values serve as model parameters. We use the set of data given in table 1 to derive those model parameters, however, the initial set could be different or expanded. We obtain two sets of elemental I-values which are optimized for the use in compounds (one set for gases, one for liquids and solids) in combination with the BAR. We use equation (10) to report uncertainty values u_{elem} for the newly determined I_{elem}. The here reported uncertainties are standard uncertainties (68% confidence interval). Some of the data used for our analysis, especially the ones used by Berger and Seltzer, are quoted for a 90% confidence interval, as reported in ICRU report 37, footnote 10. Whenever this was the case, the uncertainties were divided by a factor of 1.6 to convert from the 90% to the 68% confidence interval.

To test the validity of our data, we perform a self-consistency test. For this, we use the optimized elemental I-values to reproduce the calibration data set. The root mean square (RMS) errors between actual and predicted calibration data are compared with predicted data using ICRU-recommended elemental I-values. Again, we separate gases from liquids and solids.

2.2. Estimation of u_{BAR}

While $u_{\text{med},i}$ can be derived from experimental uncertainties, u_{BAR} needs to be estimated using a model. To estimate u_{BAR}, we use the calibration data set as listed in table 1, and calculate the residual error $\mathbf{r}$ between the estimated and experimentally measured values for $\mathbf{y}_{\text{med}}$:

$$\begin{aligned}\mathbf{r} &= \hat{\mathbf{y}}_{\text{med}} - \mathbf{y}_{\text{med}} \\ &= \mathbf{\Lambda}\left(\tilde{\mathbf{\Lambda}}_{\text{med}}^{\text{T}}\tilde{\mathbf{\Lambda}}_{\text{med}}\right)^{-1}\tilde{\mathbf{\Lambda}}_{\text{med}}^{\text{T}}\tilde{\mathbf{y}}_{\text{med}} - \mathbf{y}_{\text{med}} \\ &= \tilde{\mathbf{K}}\tilde{\mathbf{y}}_{\text{med}} - \mathbf{y}_{\text{med}} \\ &= \left(\mathbf{K} - \mathbb{1}_{N\times N}\right)\mathbf{y}_{\text{med}}\end{aligned} \tag{11}$$

with $\tilde{\mathbf{K}} = \mathbf{\Lambda}\tilde{\mathbf{M}}$ and where the elements of $\mathbf{K}$ equal the ones of $\tilde{\mathbf{K}}$ divided by the weighting factors, i.e. $\mathrm{K}_{ij} = \frac{1}{w_i}\tilde{\mathrm{K}}_{ij}$. We can now estimate the covariance matrix $\mathbf{V}(\mathbf{r})$ as

Table 1. Literature used to retrieve the *I*-values of compounds, by either dipole oscillator-strength distributions, dielectric-response functions, or measurements of the energy loss. Numbers 1–10 were used by Berger and Seltzer (1982) to assign the elemental *I*-values for the use in compounds with the BAR.

Number	Source	Year	Method	Elements involved
1	Zeiss *et al*	1977	Dipole oscillator-strength	N, H, O
2	Jhanwar *et al*	1981	Dipole oscillator-strength	H, C
3	Bichsel and Hilko	1981	α-particle beam	C, O
4	Thomas and Meath	1977	Dipole oscillator-strength	H, C
5	Thompson	1952	Proton beam	H, C, N, O, Cl
6	Nordin and Henkelmann	1979	Pion beam	H, O
7	Bader *et al*	1956	Low energy proton beam	F, Ca
8	Painter *et al*	1980	Dielectric-response functions	H, C
9	Tschalär and Bichsel	1968	Proton beam	H, C, O, Si
10	Ashley	1979	Dielectric-response functions	H, C
11	Bichsel and Hiraoka	1992	Proton beam	H, O
12	Hiraoka *et al*	1993	Proton beam	H, C, N, O, F, Cl
13	Hiraoka *et al*	1994	Proton beam	H, C, N, O, F, Cl, Si, P, Ca
14	Bichsel *et al*	2000	Carbon beam	H, O
15	Kumazaki *et al*	2007	Proton beam	H, O

$$\mathbf{V}(\mathbf{r}) = (\mathbf{K} - \mathbb{1}_{N\times N})\, V(\mathbf{y}_{\text{med}})\, (\mathbf{K} - \mathbb{1}_{N\times N})^{\text{T}} + u_{\text{BAR}}^2 \mathbb{1}_{N\times N}. \tag{12}$$

To solve for u_{BAR}^2, we find the value such that the sum of the residuals squared normalized to their variance equals its number of degrees of freedom, that is:

$$\sum_{i=1}^{N} \frac{r_i^2}{\text{V}_{ii}(r)} = N - M. \tag{13}$$

Note that the approach is based on the assumption that the experimental data for a particular element follows a Gaussian distribution. The resulting equation (13) follows a chi-square distribution with expectation value equaling its number of degrees of freedom $N - M$, N being the number of experimental data and M the number of optimized elemental *I*-values.

2.3. Application of optimal elemental *I*-values to water and reference human tissues

Using the optimized set of elemental *I*-values, we determine compound *I*-values for water and a set of 70 human reference tissues (Woodard and White 1986, White *et al* 1987). For the *I*-value of water, we need to differentiate between three different values: $I_{\text{w,BAR}}$ represents the *I*-value of water calculated with the elemental *I*-values quoted in this paper and the BAR, $I_{\text{w,ICRU37,BAR}}$ represents the *I*-value of water calculated with the ICRU 37 recommended elemental *I*-values and the BAR, and $I_{\text{w,ICRU90}}$ represents the value recently recommended by ICRU 90. The compound *I*-values are compared to the results obtained with ICRU 37 recommended values. We establish the uncertainties on compound *I*-values using the covariance matrix of the elemental *I*-values $\mathbf{V}(\hat{y}_{\text{elem}})$:

$$\mathbf{V}(\hat{y}_{\text{med}}) = \Lambda_{\text{med}} V(\hat{y}_{\text{elem}})\, \Lambda_{\text{med}}^{\text{T}}. \tag{14}$$

2.4. Uncertainties on relative stopping powers

Once the uncertainties on the mean excitation energies are determined, it is possible to propagate these into stopping power uncertainties. In this way, we quantify the uncertainty on the RSP of medium to water originating from uncertainties on *I*-values. Since the uncertainties of medium and water can be correlated depending on the water content of the medium (Yang *et al* 2012, De Smet *et al* 2018), it is important to consider covariances. Combining equations (2) and (3), the stopping number can be expressed as

$$L = \ln\left(\frac{2m_e c^2 \beta^2}{1-\beta^2}\right) - \beta^2 - \sum_{k=1}^{N} \lambda_k y_k. \tag{15}$$

The derivative of the stopping number with respect to $\ln I_i$ is then found to be

$$\frac{\partial L}{\partial y_i} = -\lambda_i. \tag{16}$$

Table 2. Comparison of elemental I-values (in eV) for the use in gas compounds. The values recommended by Berger and Seltzer (ICRU 37) are compared to the values determined with our proposed assignment scheme.

	Gases		
Element	Berger and Seltzer (1982)	This work	Uncertainty (eV)
H	19.20	21.54	0.74
C	70.00	66.75	1.08
N	82.00	79.59	1.15
O	97.00	95.17	1.01

We can now express the derivative of the RSP with respect to $\ln I_i$ as

$$\begin{aligned}\frac{\partial S}{\partial y_i} &= \rho_e \frac{\partial \frac{L_{med}}{L_w}}{\partial y_i} \\ &= \rho_e \frac{L_{med}\lambda_{w,i} - L_w\lambda_{med,i}}{L_w^2}.\end{aligned} \tag{17}$$

The variance on the RSP can now be written as using the following rule

$$\begin{aligned}V(S) &= \left(\frac{\partial S}{\partial \mathbf{y}}\right)^T V(\mathbf{y}) \left(\frac{\partial S}{\partial \mathbf{y}}\right) \\ &= \begin{pmatrix} \frac{\partial S}{\partial y_1} \\ \vdots \\ \frac{\partial S}{\partial y_N} \end{pmatrix}^T \begin{pmatrix} \mathrm{COVAR}(y_1, y_1) & & \mathrm{COVAR}(y_1, y_N) \\ \vdots & \ddots & \vdots \\ \mathrm{COVAR}(y_N, y_1) & \cdots & \mathrm{COVAR}(y_N, y_N) \end{pmatrix} \begin{pmatrix} \frac{\partial S}{\partial y_1} \\ \vdots \\ \frac{\partial S}{\partial y_N} \end{pmatrix}.\end{aligned} \tag{18}$$

2.5. Uncertainties on beam ranges

To quantify the impact on beam ranges, we perform Monte Carlo transport simulations of a pristine proton beam in homogeneous media (volume: $30 \times 30 \times 30\,\mathrm{cm}^3$). We score the energy loss and position of each interaction of the beam with the medium. We choose water and five different human reference tissues (Adipose 3, skeletal muscle 1, brain white matter, femur whole, cortical bone) relevant to proton therapy. For every material, four simulations are performed: (1) using ICRU-recommended I-values; (2) using our suggested I-values; (3) using the upper uncertainty limit and (4) using the lower uncertainty limit. For the simulations, we use the Geant4 code (Version 10.03.p02) with the QBBC physics package (Ivantchenko *et al* 2012). To calculate the energy loss in a medium, Geant4 uses the restricted Bethe formula with shell, density and higher order correction terms (i.e. the restricted Bethe–Bloch equation). We simulate proton beams of 173 MeV using 10^6 particles per beam and a 1 mm cut-off value for secondary particles.

3. Results

3.1. Optimal elemental I-values to estimate compounds I-values

The proposed approach results in a set of optimized elemental I-values for the use with the BAR with compounds. Using the same measured compound I-values than Berger and Seltzer and more recent literature on measured I-values, we calculate optimized elemental I-values for the use in gases and for the use in liquids and solids separately. Our optimized elemental I-values differ from the ones suggested by Berger and Seltzer, as tabulated in tables 2 and 3. Table 4 shows the correlation coefficients of the optimized elemental I-values for liquids and solids. We use both sets of elemental I-values to perform a self-consistency test on the calibration data. Using the ICRU 37 recommended elemental I-values suggested by Berger and Seltzer, we observe RMS errors of 1.02% (gases) and 6.17% (liquids and solids) when using the BAR to predict the underlying experimental I-values. Using our optimized elemental I-values, this prediction error can be reduced to 0.05% (gases) and 5.19% (liquids and solids). The model uncertainty arising from the BAR , i.e. u_{BAR}, is quantified as 4.42%.

3.2. Application of optimal elemental I-values to water and reference human tissues

Using our method, we estimate the compound I-value of water to $I_{w,BAR} = 78.73 \pm 2.89$ eV. This value is in good agreement with the recent recommendation given in ICRU 90 (ICRU 2014), which is based on the value $I_{w,ICRU90} = 78 \pm 2$ eV given in Andreo *et al* (2013). The compound I-values of 70 reference human tissues are listed in table 5. The uncertainty of the values suggested herein and the difference with Berger and Seltzer recommended values are also listed. In figure 1, we show the resulting uncertainties on tissue I-values when covariances are not taken into account. With our model, we obtain uncertainties between $\min\{u_{tissue}\} = 1.82$

Table 3. Comparison of elemental *I*-values in eV for the use in liquid and solid compounds. The values recommended by Berger and Seltzer (ICRU 37) are compared to the values determined with our proposed assignment scheme.

	Liquids and solids		
Element	Berger and Seltzer	This work	Uncertainty (eV)
H	19.20	22.07	1.32
C	81.00	79.91	3.61
N	82.00	77.91	3.86
O	106.00	107.44	4.88
F	112.00	136.24	6.28
Al	187.58	191.69	11.13
Si	195.50	150.47	7.60
P	195.50	199.39	42.45
Cl	180.00	175.13	7.91
Ca	215.80	258.11	16.61

Table 4. Correlation coefficients of the uncertainties of elemental *I*-values.

Element	H	C	N	O	F	Al	Si	P	Cl	Ca
H	1.00									
C	−0.12	1.00								
N	−0.02	−0.00	1.00							
O	−0.12	0.03	0.01	1.00						
F	0.04	−0.02	0.00	−0.01	1.00					
Al	0.09	−0.02	−0.01	−0.04	0.01	1.00				
Si	0.03	−0.01	−0.00	−0.01	0.00	0.01	1.00			
P	0.06	−0.02	−0.00	−0.02	0.03	0.02	0.01	1.00		
Cl	0.01	−0.01	0.00	−0.00	−0.00	0.00	0.00	0.00	1.00	
Ca	0.04	−0.02	−0.01	−0.02	−0.02	0.01	0.00	−0.35	0.01	1.00

eV (mammary gland) and $\max\{u_{\text{tissue}}\} = 3.38$ eV (cortical bone). If statistical correlations between optimized elemental *I*-values are neglected, these values increase to $\min\{u_{\text{tissue}}\} = 1.92$ eV (mammary gland) and $\max\{u_{\text{tissue}}\} = 3.85$ eV (cortical bone).

3.3. Uncertainties on relative stopping powers

We use our optimized *I*-values to calculate RSP values for 70 human reference tissues. Figure 2 shows the uncertainties on RSP values of 70 human reference tissues, arising from uncertainties on *I*-values only. We observe uncertainties on RSP values between 0.002% (mammary gland) and 0.44% (adipose tissue 3). The uncertainties observed are the smallest for the soft tissues since their water content is the highest between adipose tissue, soft tissues and bones.

3.4. Uncertainties on beam ranges

Figure 3 shows the percentage depth dose (PDD) curves for water and five human reference tissues, each using four different sets of *I*-values: (1) the ICRU-recommended values; (2) the optimized *I*-values resulting from this work, (3) the optimized *I*-values resulting from this work plus 1 standard deviation and (4) the optimized *I*-values resulting from this work minus 1 standard deviation. We observe differences in the range of the distal 80% of the maximum dose (R_{80}) between ICRU-recommended values and our values of 0.75 mm (adipose tissue 3)—1.10 mm (water using $I_{\text{w,ICRU37,BAR}}$). We find range uncertainties between 0.31% and 0.47%, with the lowest uncertainty found in femur tissue, while the highest uncertainty is found in water (see table 6).

4. Discussion

In this work, we investigate RSP and range uncertainties arising from mean excitation energies. We establish a mathematical model to optimize elemental *I*-values for the use in gases and liquids and solids with the BAR. To calculate our optimized *I*-values and establish an uncertainty budget, we utilize *I*-value and stopping power measurements from literature, most of which were used by Berger and Seltzer to establish the ICRU 37 recommended values, however we also include more recent measurements. The set of optimized elemental *I*-values for the use with the BAR in compounds and the reported uncertainties that can be used to accurately assess the uncertainties on

Table 5. Compound *I*-values determined with the elemental *I*-values recommended by Berger and Seltzer (ICRU 37) and compared to those suggested in this work. All *I*-values and standard uncertainties are given in eV.

Tissue	Berger and Seltzer	This work	Uncertainty	*I*-value difference
Adipose tissue 1	66.20	68.28	1.82 (2.67%)	2.09 (3.15%)
Adipose tissue 2	64.66	66.62	1.86 (2.79%)	1.96 (3.04%)
Adipose tissue 3	63.12	64.95	1.93 (2.98%)	1.84 (2.91%)
Adrenal gland	70.83	73.33	2.01 (2.74%)	2.50 (3.52%)
Aorta	74.78	77.50	2.34 (3.02%)	2.72 (3.64%)
Blood whole	74.78	77.62	2.47 (3.18%)	2.84 (3.79%)
Brain cerebrospinal fluid	75.52	78.93	2.89 (3.66%)	3.40 (4.51%)
Brain gray matter	74.34	77.36	2.52 (3.25%)	3.02 (4.06%)
Brain white matter	72.67	75.39	2.21 (2.92%)	2.72 (3.74%)
C4 including cartilage male	89.41	93.34	2.37 (2.53%)	3.93 (4.39%)
Cartilage	77.14	80.04	2.58 (3.22%)	2.90 (3.76%)
Clavicle scapula	92.25	96.53	2.40 (2.49%)	4.27 (4.63%)
Connective tissue	73.97	76.30	2.15 (2.82%)	2.34 (3.16%)
Cortical bone	111.63	117.81	3.38 (2.87%)	6.17 (5.53%)
Cranium	99.69	104.65	2.75 (2.63%)	4.97 (4.98%)
D6L3 including cartilage male	85.44	89.01	2.23 (2.51%)	3.58 (4.19%)
Eye lens	74.03	76.45	2.20 (2.87%)	2.42 (3.27%)
Femur Humerus spherical head	85.43	89.09	2.18 (2.45%)	3.66 (4.29%)
Femur conical trochanter	86.69	90.47	2.22 (2.45%)	3.78 (4.36%)
Femur cylindrical shaft	105.13	110.64	3.01 (2.72%)	5.51 (5.24%)
Femur total bone	90.24	94.31	2.33 (2.47%)	4.08 (4.52%)
Femur whole specimen	90.34	94.44	2.34 (2.47%)	4.10 (4.54%)
Gallbladder bile	75.03	78.23	2.69 (3.44%)	3.20 (4.26%)
Heart 1	73.43	76.13	2.27 (2.98%)	2.70 (3.67%)
Heart 2	73.91	76.72	2.37 (3.09%)	2.81 (3.80%)
Heart 3	74.61	77.52	2.49 (3.21%)	2.91 (3.91%)
Heart blood-filled	74.39	77.21	2.42 (3.14%)	2.83 (3.80%)
Humerus cylindrical shaft	93.56	97.96	2.45 (2.50%)	4.40 (4.70%)
Humerus total bone	92.23	96.50	2.40 (2.49%)	4.27 (4.63%)
Humerus whole specimen	88.06	91.98	2.26 (2.46%)	3.92 (4.45%)
Innominate female	92.82	97.08	2.45 (2.52%)	4.27 (4.60%)
Innominate male	90.75	94.80	2.37 (2.50%)	4.05 (4.46%)
Kidney 1	73.90	76.62	2.31 (3.01%)	2.72 (3.68%)
Kidney 2	74.28	77.10	2.40 (3.11%)	2.82 (3.80%)
Kidney 3	74.60	77.52	2.48 (3.20%)	2.92 (3.91%)
Liver 1	73.84	76.60	2.33 (3.04%)	2.77 (3.75%)
Liver 2	74.30	77.08	2.38 (3.09%)	2.78 (3.75%)
Liver 3	74.69	77.48	2.42 (3.12%)	2.79 (3.73%)
Lung deflated	74.72	77.59	2.48 (3.19%)	2.88 (3.85%)
Lymph	75.23	78.43	2.73 (3.48%)	3.20 (4.25%)
Mammary gland 1	66.79	68.81	1.82 (2.64%)	2.03 (3.04%)
Mammary gland 2	70.11	72.46	1.93 (2.66%)	2.35 (3.35%)
Mammary gland 3	73.84	76.53	2.31 (3.02%)	2.69 (3.65%)
Mandible	102.35	107.56	2.88 (2.67%)	5.21 (5.09%)
Muscle skeletal 1	73.74	76.40	2.28 (2.98%)	2.66 (3.60%)
Muscle skeletal 2	74.08	76.84	2.36 (3.07%)	2.75 (3.71%)
Muscle skeletal 3	74.72	77.58	2.47 (3.18%)	2.85 (3.82%)
Ovary	74.63	77.60	2.52 (3.25%)	2.97 (3.98%)
Pancreas	73.11	75.90	2.29 (3.02%)	2.79 (3.82%)
Prostate	74.70	77.67	2.54 (3.27%)	2.97 (3.97%)
Red marrow	68.81	70.94	1.83 (2.59%)	2.13 (3.10%)
Ribs 10th	95.48	100.00	2.55 (2.55%)	4.53 (4.74%)
Ribs 2nd 6th	90.33	94.37	2.35 (2.49%)	4.04 (4.47%)
Sacrum female	89.16	93.10	2.31 (2.48%)	3.93 (4.41%)

(*Continued*)

Table 5. (*Continued*)

Tissue	Berger and Seltzer	This work	Uncertainty	*I*-value difference
Sacrum male	84.25	87.71	2.15 (2.45%)	3.46 (4.11%)
Skin 1	72.43	74.82	2.06 (2.75%)	2.39 (3.30%)
Skin 2	73.35	75.87	2.18 (2.88%)	2.52 (3.44%)
Skin 3	74.06	76.74	2.31 (3.02%)	2.68 (3.62%)
Small intestine wall	74.09	77.02	2.46 (3.19%)	2.93 (3.95%)
Spleen	74.58	77.43	2.45 (3.16%)	2.85 (3.82%)
Sternum	82.03	85.28	2.09 (2.45%)	3.25 (3.96%)
Stomach	73.87	76.67	2.37 (3.10%)	2.81 (3.80%)
Testis	74.35	77.33	2.51 (3.25%)	2.98 (4.01%)
Thyroid	74.35	77.23	2.45 (3.18%)	2.88 (3.88%)
Trachea	74.44	77.20	2.38 (3.08%)	2.76 (3.71%)
Urine	75.55	78.88	2.84 (3.60%)	3.33 (4.40%)
Vertebral column C4 excluding cartilage	90.83	94.90	2.37 (2.49%)	4.07 (4.48%)
Vertebral column D6L3 excluding cartilage	86.59	90.27	2.22 (2.46%)	3.67 (4.24%)
Vertebral column whole	86.65	90.34	2.27 (2.51%)	3.70 (4.27%)
Water	75.31	78.73	2.89 (3.67%)	3.41 (4.53%)
Yellow marrow	63.78	65.66	1.89 (2.88%)	1.88 (2.95%)

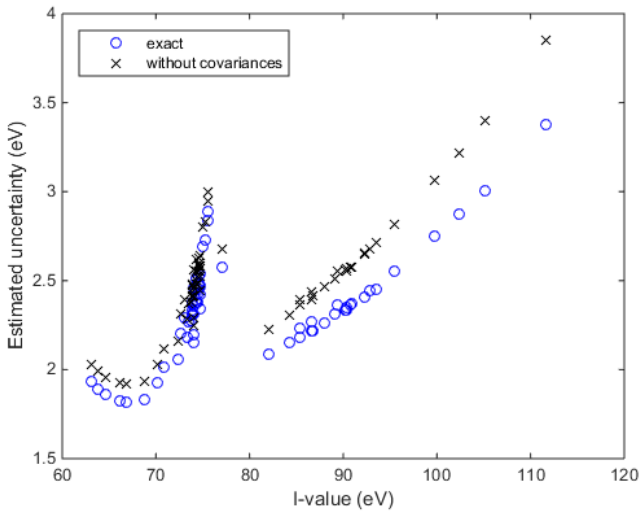

Figure 1. Calculated uncertainties on compound *I*-values for 70 human reference tissues. This graph also shows that neglecting statistical correlations between optimized elemental *I*-values leads to an overestimation of the uncertainties in compounds.

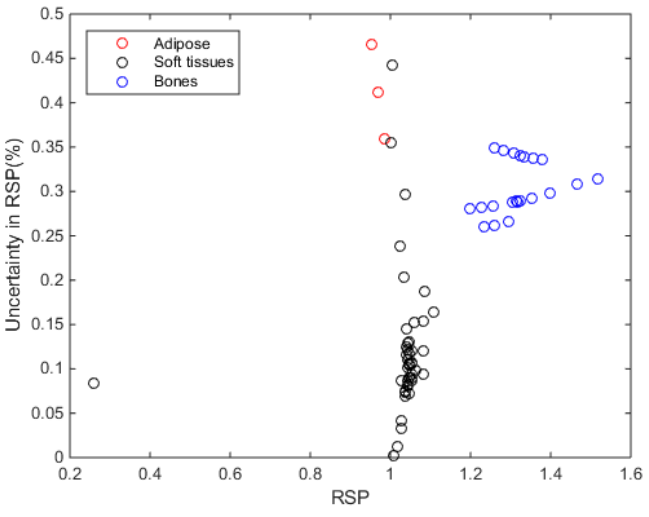

Figure 2. Calculated uncertainties on RSPs for 70 human reference tissues, arising from the uncertainties on compound *I*-values.

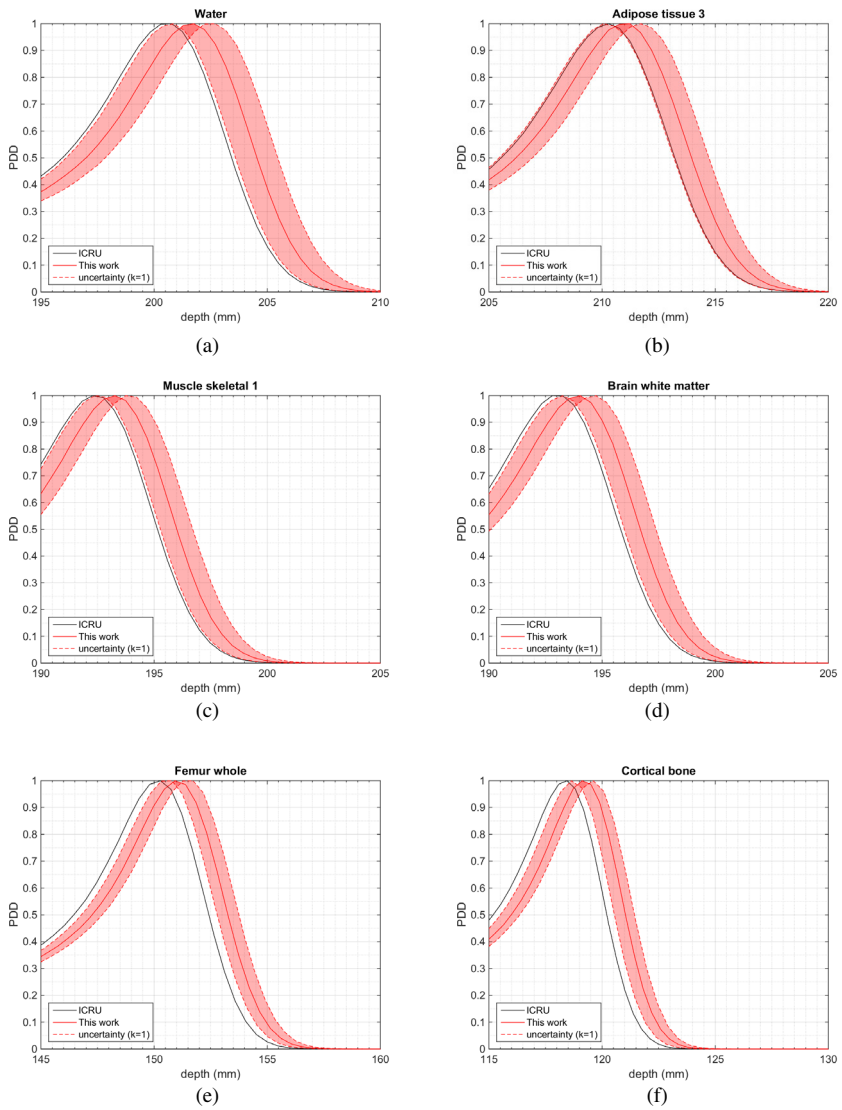

Figure 3. Percentage depth dose curves of a pristine proton beam with an initial energy of 173 MeV, simulated in homogenous media: (a) Water, (b) adipose tissue 3, (c) muscle skeletal 1, (d) brain white matter, (e) femur whole and (f) cortical bone. Shown are curves using the ICRU-recommended elemental *I*-values (black line), our suggested *I*-values (red solid line) and uncertainty limits (dashed lines). For water, the black line is simulated using the *I*-value calculated using the ICRU 37 recommended elemental *I*-values and the BAR $I_{w,ICRU37,BAR}$ to be consistent with the other media.

tissue *I*-values. Furthermore, we provide an estimation of the uncertainty coming from the BAR itself, and include this uncertainty in our model. Our model allows the propagation of uncertainties to RSP values and beam ranges, providing a better understanding of the resulting uncertainties in proton therapy treatment planning.

This study focuses on the effect of the *I*-value of a medium on the range of a particle beam and associated uncertainties. The magnitude of this effect depends on various factors such as the dose calculation algorithm and the chosen modality to determine the treatment planning inputs. A higher precision in *I*-values and their uncertainties leads to a higher precision in range prediction for both, analytical and Monte Carlo based dose calculation approaches since in both cases *I*-values are needed to calculate the stopping power using the Bethe formula.

Elemental *I*-values of liquids and solids are of special interest for proton therapy treatment planning. We propose a set of values which differs from the values recommended in ICRU 37. This is due to the fact that the underlying model used to find the optimized *I*-values differs from the methods used by Berger and Seltzer to determine the originally proposed values. For the majority of our proposed values (C, N, O, Al, P, Cl), the ICRU-recommended values are within the uncertainty budget given by our model. However, few exceptions are observed. We find considerably higher elemental *I*-values for the elements H, F, and Ca than Berger and Seltzer. In turn, our values for Si is lower. While the optimized value for P is close to the ICRU recommended value (195.5 eV versus 199.93 eV), we observe a high uncertainty of 42.45 eV. The high uncertainty can be explained due to the lack of data available for P. From the 74 liquids and solids, only 3 materials contain traces of P. The high observed uncertainty however is of little concern to clinical applications. First of all, P is only abundant as trace element in the human body. Secondly, it is only observed in bones, where we observe a strong statistical anti-correlation with Ca, compensating for the high uncertainty in P.

Table 6. Calculated beam ranges in terms of R_{80} (in mm) using Monte Carlo proton beam transport simulations. The uncertainties reported are resulting from the uncertainties on our optimized *I*-values and the differences are taken between ranges simulated with ICRU-recommended *I*-values and ranges simulated with our optimized *I*-values.

		Liquids and solids		
Material	Range ICRU	Range this work	Uncertainty (%)	Difference (%)
Water	202.25	203.35	0.95 (0.47%)	1.10 (0.54%)
Adipose tissue 3	211.97	212.72	0.79 (0.37%)	0.75 (0.35%)
Muscle skeletal 1	194.01	194.86	0.72 (0.37%)	0.85 (0.44%)
Brain white matter	194.68	195.55	0.72 (0.37%)	0.88 (0.45%)
Femur whole	151.49	152.34	0.47 (0.31%)	0.85 (0.56%)
Cortical bone	119.46	120.28	0.50 (0.42%)	0.82 (0.68%)

The calibration materials used herein are taken from various sources of literature, most of them were already utilized by Berger and Seltzer to recommend the currently clinically applied elemental *I*-values. As a self consistency study, we evaluate the accuracy of our optimized elemental *I*-values in comparison to ICRU-recommended elemental *I*-values to predict the *I*-values of the calibration material. Our optimized elemental *I*-values show a lower RMS prediction error than the ICRU-recommended values, indicating that our values are well suited to predict the *I*-values of tissues when the BAR is used. When calculating the *I*-values of 70 human reference tissues, we observe generally larger tissue *I*-values using the optimized elemental *I*-values. Using our technique and optimized elemental *I*-values, we achieve an *I*-value for water of $I_{w,BAR} = 78.73 \pm 2.89$ eV, which is in good agreement with the value recommended in the the recently published ICRU 90 report. Using the elemental *I*-values recommended in ICRU 37, the *I*-value for water is estimated as $I_{w,ICRU37,BAR} = 75.32$ eV.

Doolan *et al* (2016) tested different sets of elemental *I*-values derived with corresponding corrections to the Bethe formula. They concluded that the accuracy of the RSP values with and without corrections is equivalent as long as the correct combinations of *I*-values and corresponding corrections is used. Here, we used the Bethe formula without corrections to calculate the RSP uncertainties. If one wishes to include corrections to the formula, this could be easily incorporated into equation (2), but it is not expected to largely influence the herein quoted RSP and range uncertainties.

Our mathematical model incorporates estimates for uncertainty values associated with each optimized elemental *I*-value, and allows the propagation of uncertainties on tissue *I*-value uncertainties. We show the importance of taking into account statistical correlations between uncertainties of the different elemental *I*-values. Our analysis shows that if statistical correlations are ignored, the uncertainties might be overestimated by up to 0.5%.

The method proposed herein allows the estimation of uncertainties on tissue RSPs resulting from *I*-value uncertainties. We observe the highest RSP uncertainties in adipose tissues and bones, which is expected as those are the tissues with a low water content. Those findings were already discussed in previous studies by Yang *et al* (2012) and De Smet *et al* (2018). We observe low RSP uncertainties in soft tissues, which can be attributed to their high water content.

The resulting beam range uncertainties are assessed in water and five selected human reference tissues. We choose the tissues according to their importance to radiotherapy and abundance in the human body. Observed range uncertainties are between 0.31% and 0.47% for a 173 MeV proton beam. Overall, the ranges predicted using our optimized elemental *I*-values are systematically larger than the ranges calculated based on ICRU-recommended *I*-values. This is expected since our optimized *I*-values calculate larger tissue *I*-values than the ICRU recommendation. In our study, the observed RSP and range uncertainties are much lower than the currently assumed 1.5%.

It should be noted that the systematic shift in depth dose curves observed in the Monte Carlo simulations will not necessarily be observed with more simplistic dose calculation algorithms as implemented in treatment planning systems, since they usually use the stopping power relative to water for dose estimation. However it should be emphasized that our model yields a more realistic *I*-value for water (and closer to the recent ICRU 90 recommendation) than ICRU 37. Future work will focus on the application of optimized *I*-values to CT scans of tissues, which can potentially proof the validity and superiority of one set of elemental *I*-values over the other.

5. Conclusion

We propose a new set of optimized elemental *I*-values for the use with the Bragg additivity rule in compounds. Our mathematical model establishes an uncertainty budget on elemental *I*-values that can be propagated to compound *I*-values, accounting for experimental uncertainties as well as the uncertainty on the Bragg additivity rule itself. With our model, we provide realistic uncertainties estimations on proton RSP and beam range values in human tissues. The herein presented data show that the currently assumed range uncertainty originating from *I*-values may be overestimated. Proposed elemental *I*-values and corresponding uncertainty budgets provide evidence for a reassessment and possible reduction of those range uncertainties in clinical routine.

Acknowledgments

This work is funded by EPSRC UK (case studentship No. 20873) and the National Physical Laboratory (UK).

Appendix. Supplement data: I-values and elemental compositions used in this paper

Table A1. Gas compounds: Elemental weights and mean excitation energies of the gas compounds used in this paper. Data are taken from ICRU 37.

Compound	H	C	N	O	*I*-value (eV)	Uncertainty (eV)
Ammonia	0.1775	0.0000	0.8225	0.0000	53.7	1.1
Butane	0.1734	0.8266	0.0000	0.0000	48.3	1.0
Carbon Dioxide	0.0000	0.2729	0.0000	0.7271	85.0	1.7
Ethane	0.2011	0.7989	0.0000	0.0000	45.4	0.9
Heptane	0.1609	0.8391	0.0000	0.0000	49.2	1.0
Hexane	0.1637	0.8363	0.0000	0.0000	49.1	1.0
Methane	0.2513	0.7487	0.0000	0.0000	41.7	0.8
Nitric Oxide	0.0000	0.0000	0.4668	0.5332	87.8	1.8
Nitrous Oxide	0.0000	0.0000	0.6365	0.3635	84.9	1.7
Octane	0.1588	0.8412	0.0000	0.0000	49.5	1.0
Pentane	0.1676	0.8324	0.0000	0.0000	48.2	1.0
Propane	0.1829	0.8171	0.0000	0.0000	47.1	0.9
Water	0.1119	0.0000	0.0000	0.8881	71.6	1.4

Table A2. Liquid and solid compounds: Elemental weights and mean excitation energies of the liquid and solid compounds used in this paper. Data are taken from different sources as specified.

Compound	H	C	N	O	F	Al	Si	P	Cl	Ca	*I*-value (eV)	Uncertainty (eV)	Reference
A-150	0.1013	0.7755	0.0351	0.0523	0.0174	0.0000	0.0000	0.0000	0.0000	0.0184	65.10	10.40	ICRU (1984)
A-153	0.0000	0.5688	0.0000	0.0000	0.4312	0.0000	0.0000	0.0000	0.0000	0.0000	104.00	2.20	Hiraoka *et al* (1994)
A-174	0.1026	0.7906	0.0349	0.0000	0.0094	0.0000	0.0526	0.0000	0.0000	0.0099	71.00	1.60	Hiraoka *et al* (1994)
Acetone	0.1041	0.6204	0.0000	0.2755	0.0000	0.0000	0.0000	0.0000	0.0000	0.0000	64.20	1.90	ICRU (1984)
Adenine	0.0373	0.4444	0.5183	0.0000	0.0000	0.0000	0.0000	0.0000	0.0000	0.0000	71.40	3.60	ICRU (1984)
Aluminum Oxide	0.0000	0.0000	0.0000	0.4705	0.0000	0.5295	0.0000	0.0000	0.0000	0.0000	145.20	4.40	ICRU (1984)
Anniline	0.0758	0.7738	0.1504	0.0000	0.0000	0.0000	0.0000	0.0000	0.0000	0.0000	66.20	2.00	ICRU (1984)
B-100	0.0651	0.5424	0.0226	0.0259	0.1674	0.0000	0.0000	0.0000	0.0000	0.1766	92.00	2.00	Hiraoka *et al* (1994)
B-110	0.0355	0.3672	0.0397	0.0453	0.2493	0.0000	0.0000	0.0000	0.0000	0.2629	115.00	2.40	Hiraoka *et al* (1994)
BE-103	0.0369	0.2923	0.0119	0.3267	0.0000	0.0000	0.0000	0.1024	0.0006	0.2292	112.00	2.30	Hiraoka *et al* (1994)
BE-204	0.0511	0.4245	0.0173	0.2813	0.0000	0.0000	0.0000	0.0700	0.0009	0.1549	98.00	2.10	Hiraoka *et al* (1994)
BE-303	0.0697	0.6003	0.0245	0.2179	0.0000	0.0000	0.0000	0.0230	0.0013	0.0633	81.40	1.80	Hiraoka *et al* (1994)
Benzene	0.0774	0.9226	0.0000	0.0000	0.0000	0.0000	0.0000	0.0000	0.0000	0.0000	63.40	1.90	ICRU (1984)
Breast RMI-454	0.0868	0.6995	0.0237	0.1791	0.0000	0.0000	0.0000	0.0000	0.0014	0.0095	71.00	1.60	Hiraoka *et al* (1994)
C-552	0.0247	0.5016	0.0000	0.0045	0.4652	0.0000	0.0040	0.0000	0.0000	0.0000	95.00	2.00	Hiraoka *et al* (1994)
C10H8O4	0.0420	0.6250	0.0000	0.3330	0.0000	0.0000	0.0000	0.0000	0.0000	0.0000	75.30	1.10	Hiraoka *et al* (1993)
C16H14O3	0.0555	0.7557	0.0000	0.1888	0.0000	0.0000	0.0000	0.0000	0.0000	0.0000	76.70	1.20	Hiraoka *et al* (1993)
C2F3Cl	0.0000	0.2062	0.0000	0.0000	0.4894	0.0000	0.0000	0.0000	0.3044	0.0000	140.00	2.00	Hiraoka *et al* (1993)
C2F4	0.0000	0.2402	0.0000	0.0000	0.7598	0.0000	0.0000	0.0000	0.0000	0.0000	116.50	1.70	Hiraoka *et al* (1993)
C2H2F2	0.0315	0.3751	0.0000	0.0000	0.5934	0.0000	0.0000	0.0000	0.0000	0.0000	99.90	1.50	Hiraoka *et al* (1993)
C2H3Cl	0.0484	0.3844	0.0000	0.0000	0.0000	0.0000	0.0000	0.0000	0.5672	0.0000	105.60	1.60	Hiraoka *et al* (1993)
C2H4	0.1437	0.8563	0.0000	0.0000	0.0000	0.0000	0.0000	0.0000	0.0000	0.0000	61.00	0.90	Hiraoka *et al* (1993)
C3H6	0.1437	0.8563	0.0000	0.0000	0.0000	0.0000	0.0000	0.0000	0.0000	0.0000	61.50	0.90	Hiraoka *et al* (1993)
C5H8O2	0.0557	0.6161	0.0000	0.3283	0.0000	0.0000	0.0000	0.0000	0.0000	0.0000	74.60	1.10	Hiraoka *et al* (1993)
C5H8O2	0.0557	0.6161	0.0000	0.3283	0.0000	0.0000	0.0000	0.0000	0.0000	0.0000	73.70	1.10	Hiraoka *et al* (1993)
C6H11ON	0.0980	0.6368	0.1238	0.1414	0.0000	0.0000	0.0000	0.0000	0.0000	0.0000	71.60	1.10	Hiraoka *et al* (1993)
C6H12	0.1437	0.8563	0.0000	0.0000	0.0000	0.0000	0.0000	0.0000	0.0000	0.0000	62.40	0.90	Hiraoka *et al* (1993)
C8H8	0.0774	0.9226	0.0000	0.0000	0.0000	0.0000	0.0000	0.0000	0.0000	0.0000	67.70	1.00	Hiraoka *et al* (1993)
CH2O	0.0671	0.4000	0.0000	0.5329	0.0000	0.0000	0.0000	0.0000	0.0000	0.0000	84.20	1.30	Hiraoka *et al* (1993)

(*Continued*)

Table A2. (*Continued*)

Compound	H	C	N	O	F	Al	Si	P	Cl	Ca	*I*-value (eV)	Uncertainty (eV)	Reference
Calcium Flouride	0.0000	0.0000	0.0000	0.0000	0.4867	0.0000	0.0000	0.0000	0.0000	0.5133	166.00	13.30	ICRU (1984)
Carbon Tetrachloride	0.0000	0.0781	0.0000	0.0000	0.0000	0.0000	0.0000	0.0000	0.9219	0.0000	166.30	5.00	ICRU (1984)
Chlorobenzene	0.0448	0.6402	0.0000	0.0000	0.0000	0.0000	0.0000	0.0000	0.3150	0.0000	89.10	2.80	ICRU (1984)
Chloroform	0.0084	0.1006	0.0000	0.0000	0.0000	0.0000	0.0000	0.0000	0.8910	0.0000	156.00	4.70	ICRU (1984)
Cyclohexane	0.1437	0.8563	0.0000	0.0000	0.0000	0.0000	0.0000	0.0000	0.0000	0.0000	56.40	1.70	ICRU (1984)
Dichlorobenzene	0.0274	0.4902	0.0000	0.0000	0.0000	0.0000	0.0000	0.0000	0.4823	0.0000	106.50	3.20	ICRU (1984)
Dichlorodiethyl Ether	0.0564	0.3359	0.0000	0.1119	0.0000	0.0000	0.0000	0.0000	0.4958	0.0000	103.30	4.10	ICRU (1984)
Dichloroethane	0.0407	0.2427	0.0000	0.0000	0.0000	0.0000	0.0000	0.0000	0.7166	0.0000	111.90	4.50	ICRU (1984)
Diethyl Ether	0.1360	0.6482	0.0000	0.2158	0.0000	0.0000	0.0000	0.0000	0.0000	0.0000	60.00	1.80	ICRU (1984)
Ethyl Alcohol	0.1313	0.5214	0.0000	0.3473	0.0000	0.0000	0.0000	0.0000	0.0000	0.0000	62.90	1.90	ICRU (1984)
Fat RMI-453	0.0836	0.6914	0.0236	0.1693	0.0307	0.0000	0.0000	0.0000	0.0014	0.0000	72.30	1.60	Hiraoka *et al* (1994)
Glycerol	0.0875	0.3910	0.0000	0.5215	0.0000	0.0000	0.0000	0.0000	0.0000	0.0000	72.60	2.20	ICRU (1984)
Guanine	0.0333	0.3974	0.4634	0.1059	0.0000	0.0000	0.0000	0.0000	0.0000	0.0000	75.00	3.80	ICRU (1984)
Hard bone RMI-450	0.0310	0.3126	0.0099	0.3757	0.0000	0.0000	0.0000	0.0000	0.0005	0.2703	114.00	2.40	Hiraoka *et al* (1994)
Inner bone RMI-456	0.0790	0.6379	0.0423	0.0988	0.0000	0.0000	0.0000	0.0000	0.1420	0.0000	81.00	1.80	Hiraoka *et al* (1994)
Methanol	0.1258	0.3748	0.0000	0.4993	0.0000	0.0000	0.0000	0.0000	0.0000	0.0000	67.60	2.00	ICRU (1984)
Muscle RMI-452	0.0841	0.6797	0.0227	0.1887	0.0000	0.0000	0.0000	0.0000	0.0013	0.0235	75.00	1.60	Hiraoka *et al* (1994)
Nitrobenzene	0.0409	0.5854	0.1138	0.2599	0.0000	0.0000	0.0000	0.0000	0.0000	0.0000	75.80	2.30	ICRU (1984)
Nylon	0.0980	0.6368	0.1238	0.1414	0.0000	0.0000	0.0000	0.0000	0.0000	0.0000	63.90	3.80	ICRU (1984)
Parrafin Wax	0.1486	0.8514	0.0000	0.0000	0.0000	0.0000	0.0000	0.0000	0.0000	0.0000	48.30	3.40	ICRU (1984)
Polyethylene	0.1437	0.8563	0.0000	0.0000	0.0000	0.0000	0.0000	0.0000	0.0000	0.0000	57.40	4.60	ICRU (1984)
Polymethyl Methacrylate	0.0805	0.5999	0.0000	0.3196	0.0000	0.0000	0.0000	0.0000	0.0000	0.0000	74.00	3.00	ICRU (1984)
Polystyrene	0.0774	0.9226	0.0000	0.0000	0.0000	0.0000	0.0000	0.0000	0.0000	0.0000	68.70	2.70	ICRU (1984)
Polytetrafluoro-ethylene	0.0000	0.2402	0.0000	0.0000	0.7598	0.0000	0.0000	0.0000	0.0000	0.0000	99.10	5.90	ICRU (1984)

(*Continued*)

Table A2. (*Continued*)

Compound	H	C	N	O	F	Al	Si	P	Cl	Ca	*I*-value (eV)	Uncertainty (eV)	Reference
Pyridine	0.0637	0.1771	0.7592	0.0000	0.0000	0.0000	0.0000	0.0000	0.0000	0.0000	66.20	2.00	ICRU (1984)
Silicon Dioxide	0.0000	0.0000	0.0000	0.2217	0.0000	0.0000	0.7783	0.0000	0.0000	0.0000	139.20	4.20	ICRU (1984)
Solid water	0.0809	0.6722	0.0240	0.1984	0.0000	0.0000	0.0000	0.0000	0.0013	0.0232	73.30	1.60	Hiraoka *et al* (1994)
Styrene	0.0774	0.9226	0.0000	0.0000	0.0000	0.0000	0.0000	0.0000	0.0000	0.0000	64.00	1.90	ICRU (1984)
TEP-NIRS	0.1010	0.7890	0.0350	0.0400	0.0170	0.0000	0.0000	0.0000	0.0000	0.0180	69.40	1.50	Hiraoka *et al* (1994)
Tetrachloroethylene	0.0000	0.1449	0.0000	0.0000	0.0000	0.0000	0.0000	0.0000	0.8551	0.0000	159.20	4.80	ICRU (1984)
Toluene	0.0873	0.9127	0.0000	0.0000	0.0000	0.0000	0.0000	0.0000	0.0000	0.0000	62.50	1.90	ICRU (1984)
Trichloroethylene	0.0008	0.1841	0.0000	0.0000	0.0000	0.0000	0.0000	0.0000	0.8151	0.0000	148.10	4.40	ICRU (1984)
WE-211	0.0820	0.6626	0.0220	0.2071	0.0000	0.0000	0.0000	0.0000	0.0037	0.0226	72.00	1.60	Hiraoka *et al* (1994)
Water Bichsel	0.1119	0.0000	0.0000	0.8881	0.0000	0.0000	0.0000	0.0000	0.0000	0.0000	79.70	0.50	Bichsel and Hiraoka (1992)
Water Bichsel 2	0.1119	0.0000	0.0000	0.8881	0.0000	0.0000	0.0000	0.0000	0.0000	0.0000	80.00	1.30	Bichsel *et al* (2000)
Water Emfietzoglou	0.1119	0.0000	0.0000	0.8881	0.0000	0.0000	0.0000	0.0000	0.0000	0.0000	77.80	1.00	Emfietzoglou *et al* (2009)
Water Kumazaki	0.1119	0.0000	0.0000	0.8881	0.0000	0.0000	0.0000	0.0000	0.0000	0.0000	78.40	1.00	Kumazaki *et al* (2007)
Water Nordin	0.1119	0.0000	0.0000	0.8881	0.0000	0.0000	0.0000	0.0000	0.0000	0.0000	74.60	2.70	Nordin and Henkelman (1979)
Water Thompson	0.1119	0.0000	0.0000	0.8881	0.0000	0.0000	0.0000	0.0000	0.0000	0.0000	75.40	1.90	Thompson (1952)
Xylene	0.1118	0.8882	0.0000	0.0000	0.0000	0.0000	0.0000	0.0000	0.0000	0.0000	61.80	1.90	ICRU (1984)
n-Butyl Alcohol	0.1360	0.6481	0.0000	0.2159	0.0000	0.0000	0.0000	0.0000	0.0000	0.0000	59.90	1.80	ICRU (1984)
n-Heptane	0.1609	0.8391	0.0000	0.0000	0.0000	0.0000	0.0000	0.0000	0.0000	0.0000	54.40	1.60	ICRU (1984)
n-Hexane	0.1637	0.8363	0.0000	0.0000	0.0000	0.0000	0.0000	0.0000	0.0000	0.0000	54.00	1.60	ICRU (1984)
n-Penthane	0.1676	0.8324	0.0000	0.0000	0.0000	0.0000	0.0000	0.0000	0.0000	0.0000	53.60	1.60	ICRU (1984)
n-Propyl Alcohol	0.1342	0.5996	0.0000	0.2662	0.0000	0.0000	0.0000	0.0000	0.0000	0.0000	61.10	1.80	ICRU (1984)

ORCID iDs

Arthur Lalonde https://orcid.org/0000-0002-8715-8235

References

Alvarez R and Macovski A 1976 Energy-selective reconstructions in x-ray computerised tomography *Phys. Med. Biol.* **21** 733

Andreo P 2009 On the clinical spatial resolution achievable with protons and heavier charged particle radiotherapy beams *Phys. Med. Biol.* **54** N205

Andreo P, Wulff J, Burns D and Palmans H 2013 Consistency in reference radiotherapy dosimetry: resolution of an apparent conundrum when 60co is the reference quality for charged-particle and photon beams *Phys. Med. Biol.* **58** 6593

Ashley J, Tung C and Ritchie R 1978 Inelastic interactions of electrons with polystyrene: calculations of mean free paths, stopping powers, and csda ranges *IEEE Trans. Nucl. Sci.* **25** 1566–70

Bader M, Pixley R, Mozer F and Whaling W 1956 Stopping cross section of solids for protons, 50–600 kev *Phys. Rev.* **103** 32

Bär E, Lalonde A, Royle G, Lu H M and Bouchard H 2017 The potential of dual-energy CT to reduce proton beam range uncertainties *Med. Phys.* **44** 2332–44

Bär E, Lalonde A, Zhang R, Jee K W, Yang K, Sharp G, Liu B, Royle G, Bouchard H and Lu H M 2018 Experimental validation of two dual-energy CT methods for proton therapy using heterogeneous tissue samples *Med. Phys.* **45** 48–59

Bazalova M, Carrier J F, Beaulieu L and Verhaegen F 2008 Dual-energy CT-based material extraction for tissue segmentation in Monte Carlo dose calculations *Phys. Med. Biol.* **53** 2439

Berger M J and Seltzer S M 1982 Stopping powers and ranges of electrons and positions (No. NBSIR-82-2550) (National Standard Reference System)

Besemer A, Paganetti H and Bednarz B 2013 The clinical impact of uncertainties in the mean excitation energy of human tissues during proton therapy *Phys. Med. Biol.* **58** 887

Bethe H 1930 Zur theorie des durchgangs schneller korpuskularstrahlen durch materie *Ann. Phys.* **397** 325–400

Bichsel H and Hilko R 1981 Measurement of the energy loss of alpha particles in carbon dioxide *Helv. Phys. Acta* **53** 655

Bichsel H and Hiraoka T 1992 Energy loss of 70 MeV protons in elements *Nucl. Instrum. Methods Phys. Res. Sect.* B **66** 345–51

Bichsel H, Hiraoka T and Omata K 2000 Aspects of fast-ion dosimetry *Radiat. Res.* **153** 208–19

Bourque A, Carrier J F and Bouchard H 2014 A stoichiometric calibration method for dual energy computed tomography *Phys. Med. Biol.* **59** 2059

De Smet V, Labarbe R, Vander Stappen F, Macq B and Sterpin E 2018 Reassessment of stopping power ratio uncertainties caused by mean excitation energies using a water-based formalism *Med. Phys.* **45** 3361–70

Doolan P, Collins-Fekete C A, Dias M, Ruggieri T A, D'Souza D and Seco J 2016 Inter-comparison of relative stopping power estimation models for proton therapy *Phys. Med. Biol.* **61** 8085

Emfietzoglou D, Garcia-Molina R, Kyriakou I, Abril I and Nikjoo H 2009 A dielectric response study of the electronic stopping power of liquid water for energetic protons and a new I-value for water *Phys. Med. Biol.* **54** 3451

Hiraoka T, Kawashima K, Hoshino K and Bichsel H 1994 Energy loss of 70 MeV protons in tissue-substitute materials *Phys. Med. Biol.* **39** 983

Hiraoka T, Kawashima K, Hoshino K, Fukumura A and Bichsel H 1993 Energy loss of 70 mev protons in organic polymers *Med. Phys.* **20** 135–41

Hünemohr N, Krauss B, Tremmel C, Ackermann B, Jäkel O and Greilich S 2014a Experimental verification of ion stopping power prediction from dual energy CT data in tissue surrogates *Phys. Med. Biol.* **59** 83

Hünemohr N, Paganetti H, Greilich S, Jäkel O and Seco J 2014b Tissue decomposition from dual energy CT data for MC based dose calculation in particle therapy *Med. Phys.* **41** 061714

ICRU 1984 *Stopping Powers for Electrons and Positrons* (*ICRU Report* vol 37) (Bethesda, MD: International Commission on Radiation Units and Measurements)

ICRU 1993 *Stopping Powers and Ranges for Protons and Alpha Particles* (*ICRU Report* vol 49) (Bethesda, MD: International Commission on Radiation Units and Measurements)

ICRU 2014 *Key Data for Ionizing-Radiation Dosimetry: Measurement Standards and Applications* (*ICRU Report* vol 90) (Bethesda, MD: International Commission on Radiation Units and Measurements)

Ivantchenko A, Ivanchenko V, Quesada Molina J M and Incerti S 2012 Geant4 hadronic physics for space radiation environment *Int. J. Radiat. Biol.* **88** 171–5

Jhanwar B, Meath W and MacDonald J 1981 Dipole oscillator strength distributions and sums for C2H6, C3H8, n-C4H10, n-C5H12, n-C6H14, n-C7H16, and n-C8H18 *Can. J. Phys.* **59** 185–97

Kumazaki Y, Akagi T, Yanou T, Suga D, Hishikawa Y and Teshima T 2007 Determination of the mean excitation energy of water from proton beam ranges *Radiat. Meas.* **42** 1683–91

Lalonde A, Bär E and Bouchard H 2017 A Bayesian approach to solve proton stopping powers from noisy multi-energy CT data *Med. Phys.* **44** 5293–302

Lalonde A, Bär E and Bouchard H 2017 A Bayesian approach to solve proton stopping powers from noisy multi-energy CT data *Med. Phys.*

Landry G, Parodi K, Wildberger J and Verhaegen F 2013 Deriving concentrations of oxygen and carbon in human tissues using single-and dual-energy CT for ion therapy applications *Phys. Med. Biol.* **58** 5029

Möhler C, Russ T, Wohlfahrt P, Elter A, Runz A, Richter C and Greilich S 2018 Experimental verification of stopping-power prediction from single-and dual-energy computed tomography in biological tissues *Phys. Med. Biol.* **63** 025001

Möhler C, Wohlfahrt P, Richter C and Greilich S 2016 Range prediction for tissue mixtures based on dual-energy CT *Phys. Med. Biol.* **61** N268

Nordin J and Henkelman R 1979 Measurement of stopping power ratios for 60 MeV positive or negative pions *Phys. Med. Biol.* **24** 781

Paganetti H 2012 Range uncertainties in proton therapy and the role of Monte Carlo simulations *Phys. Med. Biol.* **57** R99

Painter L, Arakawa E, Williams M and Ashley J 1980 Optical properties of polyethylene: measurement and applications *Radiat. Res.* **83** 1–18

Paul H and Sánchez-Parcerisa D 2013 A critical overview of recent stopping power programs for positive ions in solid elements *Nucl. Instrum. Methods Phys. Res. Sect.* B **312** 110–7

Sánchez-Parcerisa D, Gemmel A, Jäkel O, Parodi K and Rietzel E 2012 Experimental study of the water-to-air stopping power ratio of monoenergetic carbon ion beams for particle therapy *Phys. Med. Biol.* **57** 3629

Schaffner B and Pedroni E 1998 The precision of proton range calculations in proton radiotherapy treatment planning: experimental verification of the relation between CT-HU and proton stopping power *Phys. Med. Biol.* **43** 1579
Schneider U, Pedroni E and Lomax A 1996 The calibration of CT Hounsfield units for radiotherapy treatment planning *Phys. Med. Biol.* **41** 111
Schneider W, Bortfeld T and Schlegel W 2000 Correlation between CT numbers and tissue parameters needed for monte carlo simulations of clinical dose distributions *Phys. Med. Biol.* **45** 459
Sudhyadhom A 2017 Determination of mean ionization potential using magnetic resonance imaging for the reduction of proton beam range uncertainties: theory and application *Phys. Med. Biol.* **62** 8521
Taasti V *et al* 2018 Inter-centre variability of CT-based stopping-power prediction in particle therapy: survey-based evaluation *Phys. Imaging Radiat. Oncol.* **6** 25–30
Taasti V, Michalak G, Hansen D, Deisher A, Kruse J, Krauss B, Muren L, Petersen J and McCollough C 2017 Validation of proton stopping power ratio estimation based on dual energy CT using fresh tissue samples *Phys. Med. Biol.* **63** 015012
Taasti V, Petersen J B, Muren L, Thygesen J and Hansen D 2016 A robust empirical parametrization of proton stopping power using dual energy CT *Med. Phys.* **43** 5547–60
Thomas G F and Meath W 1977 Dipole spectrum, sums and properties of ground-state methane and their relation to the molar refractivity and dispersion energy constant *Mol. Phys.* **34** 113–25
Thompson T J 1952 Effect of chemical structure on stopping powers for high-energy Protons *Thesis* (No. UCRL-1910) Radiation Lab., University of California Berkeley
Torikoshi M, Tsunoo T, Sasaki M, Endo M, Noda Y, Ohno Y, Kohno T, Hyodo K, Uesugi K and Yagi N 2003 Electron density measurement with dual-energy x-ray CT using synchrotron radiation *Phys. Med. Biol.* **48** 673
Tschalär C and Bichsel H 1968 Mean excitation potential of light compounds *Phys. Rev.* **175** 476
White D, Woodard H and Hammond S 1987 Average soft-tissue and bone models for use in radiation dosimetry *Br. J. Radiol.* **60** 907–13
Williamson J, Li S, Devic S, Whiting B and Lerma F 2006 On two-parameter models of photon cross sections: application to dual-energy CT imaging *Med. Phys.* **33** 4115–29
Woodard H and White D 1986 The composition of body tissues *Br. J. Radiol.* **59** 1209–18
Xie Y, Ainsley C, Yin L, Zou W, McDonough J, Solberg T D, Lin A and Teo B K K 2018 *Ex vivo* validation of a stoichiometric dual energy CT proton stopping power ratio calibration *Phys. Med. Biol.* **63** 055016
Yang M, Virshup G, Clayton J, Zhu X, Mohan R and Dong L 2010 Theoretical variance analysis of single-and dual-energy computed tomography methods for calculating proton stopping power ratios of biological tissues *Phys. Med. Biol.* **55** 1343
Yang M, Zhu X, Park P, Titt U, Mohan R, Virshup G, Clayton J and Dong L 2012 Comprehensive analysis of proton range uncertainties related to patient stopping-power-ratio estimation using the stoichiometric calibration *Phys. Med. Biol.* **57** 4095
Zeiss G, Meath W J, MacDonald J and Dawson D 1977 Accurate evaluation of stopping and straggling mean excitation energies for N, O, H_2, N_2, O_2, NO, NH_3, H_2O, and N_2O using dipole oscillator strength distributions: a test of the validity of Bragg's rule *Radiat. Res.* **70** 284–303
Zhang R, Taddei P J, Fitzek M M and Newhauser W D 2010 Water equivalent thickness values of materials used in beams of protons, helium, carbon and iron ions *Phys. Med. Biol.* **55** 2481